Chemical Engineering Journal 339 (2018) 296–302

Contents lists available at ScienceDirect

Chemical Engineering Journal

journal homepage: www.elsevier.com/locate/cej

Adsorption of estrogen contaminants (17β-estradiol and 17α-ethynylestradiol) by graphene nanosheets from water: Effects of graphene characteristics and solution chemistry

Luhua Jiang[a,b], Yunguo Liu[a,b,*], Guangming Zeng[a,b], Shaobo Liu[c], Xinjiang Hu[d], Lu Zhou[e], Xiaofei Tan[a,b], Ni Liu[a,b], Meifang Li[a,b], Jun Wen[f]

[a] College of Environmental Science and Engineering, Hunan University, Changsha 410082, PR China
[b] Key Laboratory of Environmental Biology and Pollution Control (Hunan University), Ministry of Education, Changsha 410082, PR China
[c] School of Metallurgy and Environment, Central South University, Changsha 410083, PR China
[d] College of Environmental Science and Engineering Research, Central South University of Forestry and Technology, Changsha 410004, PR China
[e] School of Hydraulic Engineering, Changsha University of Science and Technology, Changsha, Hunan 410004, PR China
[f] College of Agriculture, Guangxi University, Nanning 530005, PR China

HIGHLIGHTS

- Estrogens adsorption of rGOs were significantly increased with increasing reduction degree.
- π-π stacking interaction could be considered as a predominant interaction to the enhanced adsorption capacities of rGOs.
- The presence of NOM suppressed estrogens adsorption to rGOs.
- Represented pH effect on sorption were correlated with hydrophobic interaction, electrostatic repulsion, and H-bonding.
- Changing ionic strength IS had negligible effect on estrogen adsorption.

ARTICLE INFO

Keywords:
Estrogen contaminants
Graphene nanosheets
Reduction degree
Natural organic matter

ABSTRACT

In this research, adsorption of two estrogens, namely, 17β-estradiol (E2) and 17α-ethynylestradiol (EE2), by graphene nanosheets with different reduction degrees (rGOs) were investigated; and the effects of solution chemistry, such as natural organic matter (NOM), pH and ionic strength (IS), on the E2 and EE2 adsorption behaviors were also examined. Results indicated that adsorption abilities of estrogens increased with increasing the reduction degree of rGOs; the π–π stacking interaction could be considered as a predominant interaction to the enhanced adsorption capacities of rGOs. Among the solution chemistry, NOM exhibited the significant influence on estrogens adsorption, which suggested that once released into water environments, graphene materials will adsorb estrogens but with a lower adsorption ability than that in ultrapure water due to the ubiquitous presence of NOM in aquatic environments. Besides, estrogens adsorption on rGOs was pH-dependent, but the influence of acid rain would be insignificant due to slight change in low pH range. However, IS within the typical range in natural waters did not exhibit significant influence on the uptake of estrogens by rGOs. Above findings of this work might have significant implications for the fate and transport of estrogens with graphene materials in the environment.

1. Introduction

As known, graphene nanosheets are two-dimensional, planar sheets with a single atomic layer of sp^2-hybridized carbon arranged in a honeycomb structure, and can serve as a basic building stone for carbon materials such as fullerene and nanotubes [1,2]. The unique structure endows graphene materials with outstanding physical and chemical properties, which make them ideal candidates for many potential applications ranging from photonics devices, electronic devices, sensors, biomedicines, contaminations adsorption [3–10]. Over the next decades, commercial production and industrial scale application of graphene materials are expected to grow exponentially [11]. Therefore, a

* Corresponding author at: College of Environmental Science and Engineering, Hunan University, Changsha 410082, PR China.
E-mail address: liuyunguo_hnu@163.com (Y. Liu).

https://doi.org/10.1016/j.cej.2017.12.034
Received 21 October 2017; Received in revised form 5 December 2017; Accepted 6 December 2017
Available online 12 December 2017
1385-8947/

mass of graphene materials will be produced and used in the future, which will result in the release of graphene materials into the environment and then lead to various health and environmental risks for plants, animals and humans [12–14]. Estrogens, as the unique environmental concern among endocrine disrupting chemicals, can be capable of triggering fish egg production inhibition, sex reversal of males, and even collapse of local fish populations [15]. Recently, estrogens were widely detected in surface and ground waters as well as in tap waters [16–19]. Discharge of domestic sewage effluents is considered as one of the main sources of estrogens in the aquatic environments, and the disposal of animal wastes also released significant amounts of estrogens into soil and groundwater [20,21]. Until now, many studies have revealed that graphene materials with large specific surface areas, abundant functional groups, and strong π–π interactions possessed strong affinity to estrogen contaminants [22–27]. Thus, the adsorption behavior of graphene materials may affect the fate and transport of estrogens and finally pose greater environmental risks; and the acquaintance of estrogen adsorption onto graphene materials is essential for investigating the effect of graphene materials on the fate and transport of estrogens and for developing a novel adsorbent for estrogen pollutants.

It is already well known that the affinity of graphene materials can be mainly ascribed to two parts: the oxygen-containing functional groups and the aromatic matrix [28,29]. The oxygen-containing functional groups, such as carboxyl groups at the edges, hydroxyl groups, and epoxy groups in the basal plane [30], lead graphene materials to extreme hydrophilicity with high negative-charge density. Wu et al. demonstrated that methylene blue strongly adsorbed on graphene material surface through electrostatic attraction and hydrogen band, yielding an adsorption capacity of 529.10 mg/g [31]. In addition, graphene materials have potential applications in eliminating the organic pollutants containing benzene ring(s) due to the strong interaction between the π system of aromatic matrix of graphene and the π system of the target pollutants. Xu et al. reported that the high affinity of the polycyclic aromatic hydrocarbons to graphene materials was dominated by π–π stacking [32]. Thus, the interactions between graphene materials and contaminants are closely related to the structure and properties of graphene materials. As reported, by varying the reduction degree of graphene oxide nanosheets could significantly alter their physiochemical properties [30]. Nevertheless, few work concentrated on the possible correlations between the adsorption ability of estrogen contaminates and reduction degree of graphene oxide nanosheets. In addition, adsorption can be greatly influenced by the background chemistry; the existing formations of organic chemicals in solution are highly pH dependent; ions (i.e. Na^+, and Ca^{2+}) may generate a "squeezing-out" and/or "salting-out" effect on uptake of hydrophobic organics; the natural organic matter (NOM) may also have severe influences on adsorption due to its two opposite effects: reducing adsorption sites via direct competition and pore blockage or increasing adsorption sites ascribed to its better dispersibility [33–35].

In this work, therefore, four graphene with different reduction degrees were synthesized successfully through reducing graphene oxide (GO) with different reduction duration and dose of reductant, and then employed in the removal of two selected estrogens from aqueous solution, namely, 17β-estradiol (E2) and 17α-ethynyl estradiol (EE2). Subsequently, the adsorption performance of E2 and EE2 by obtained reduced graphene samples (rGOs) in ultrapure water and NOM solution were examined. Besides, bath adsorption experiments were also systematically conducted under various initial pH values and ionic strength (IS) levels.

2. Experimental section

2.1. Chemical reagents

The materials for preparation of graphene (i.e., graphite, sulfuric acid, sodium nitrate, potassium permanganate, and ascorbic acid) were all analytical reagent grade and purchased from Shanghai Chemical Corp (Shanghai, China). E2 (98%) and EE2 (98%) were purchased from Sigma-Aldrich Chemical Corporation, USA. Molecular structures and selected physiochemical parameters of E2 and EE2 are listed in Fig. S1 and Table S1 in Supporting information, respectively. Besides, the detail description of NOM solution was also shown in the Supporting information.

2.2. Preparation of graphene with different reduction degrees

GO was prepared according to the previous publications of our group [36,37]. rGO were synthesized by using the hydrazine hydrate to reduce GO [38]. Briefly, a 1 L GO solution (2 mg/mL) was ultrasonicated 2 h, then centrifuged 5 min at 3000 rpm to remove any unpeeled sheets. The solution pH was adjusted to 10.0 via adding 28% ammonia solution. Then, a certain volume of hydrazine hydrate (80 wt %) was added, and the solution was heated at 98 °C in a water bath under a water-cooled condenser for a certain time. The black solution was filtered through a 0.22 μm membrane filter, and washed completely with ultrapure water and methanol to remove the excess hydrazine. Finally after freeze dried, the powder-like rGO was obtained. With variations in the dose of reductant and the reduction time in above preparation process, four rGOs with different reduction degrees have been successfully obtained and named as $rGO_{1\text{-}4}$ respectively. The detailed preparation conditions are illustrated in Table 1.

2.3. General characterization

Several techniques have been applied in the characterization of samples. Raman spectra was measured using a Raman spectrometer (Jobin Yvon LabRam-010, France) with 532 nm excitation wavelength. Wide-angle X-ray powder diffraction (XRD, Bruker AXS, D8 ADVANCE) was carried out to characterize the crystalline phases using Cu-Kα radiation (λ = 0.15418 nm). X-ray photoelectron spectroscopy (XPS) was recorded using an ESCALAB 250Xi X-ray photoelectron spectrometer (Thermo Fisher, USA) with the scanning range of 0–1000 eV. The chemical composition (C, and O) was measured using an elemental analyzer (Vario EL III, Elementar, Germany). pH of the point of zero charge (pH_{PZC}) was investigated through pH equilibration technique. Electron microscopy images were taken by a high-resolution transmission electron microscope (HR-TEM, JEM-2100F) to identify the morphology and microscopic structure of samples. The Brunauer-Emmett-Teller (BET) surface areas and pore size distributions were characterized using nitrogen physisorption data at 77 K obtained with automatic surface analyzer (ASAP 2020 M + C, Micromeritics Co., USA); the BET equation was used to calculate specific surface area (SSA_{BET}); the total pore volumes (PV_T) were obtained from the adsorbed volume of nitrogen near the saturation point (P/P_o = 0.99); pore size distributions

Table 1
Preparation conditions and selected properties of the rGOs.

Adsorbent		rGO_1	rGO_2	rGO_3	rGO_4
Reduce time (h)		4	4	8	16
Hydrazine dose (mL)		5	10	15	20
Aromatic cluster size (nm)		2.87	3.07	3.18	3.31
Content of graphitic zones (G%)		26.1	32.8	42.5	59.1
Content of sp^2 clusters in oxidized zones (a%)		22.6	24.1	26.3	27.7
SSA_{BET} (m^2/g)		342	247	210	153
PV_T (cm^3/g)		0.186	0.155	0.145	0.109
PSD	V_{micro} (< 2 nm)%	0.7	0.6	0.5	0.3
	V_{meso} (2–50 nm)%	68.5	67.6	65.1	60.7
	V_{macro} (> 50 nm)%	30.8	31.8	34.4	39.0
Oxygen content %		23.94	18.11	15.21	12.60
C/O atomic ratio		2.94	4.35	5.26	6.67
pH_{pzc}		3.8	4.3	4.8	5.2

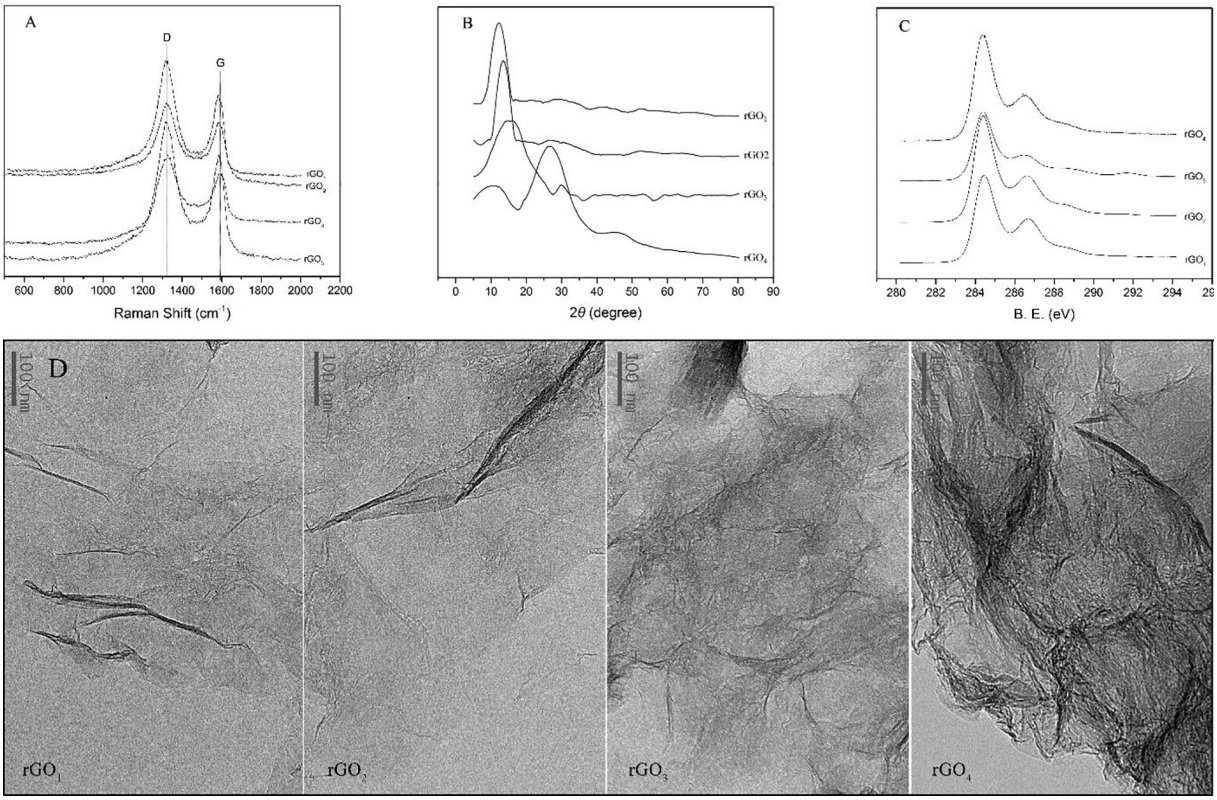

Fig. 1. Photographs of (A) Raman spectra, (B) XRD patterns, (C) XPS spectra, and (D) HR-TEM images of rGOs.

(PSD) of rGOs were obtained from the nitrogen isotherms through the Density Functional Theory (DFT) model.

2.4. Adsorption experiments

Constant dose bottle point batch adsorption isotherms were performed in 250 mL amber glass bottles with Teflon lined screw caps. Two types of isotherms were carried out at room temperature (25 ± 1 °C):

(1) Ultrapure water experiments: Each estrogen was dissolved in methanol to prepare the concentrated stock solution, respectively. Bottles containing about 1 mg of samples were initially half filled with ultrapure water. After sonicated for 30 min, bottles were completely filled with ultrapure water prior to spiking predetermined volumes of estrogens methanol stock solution. Meanwhile, the volume of methanol in the spiked solution was maintained at less than 0.1% to minimize the co-solvent effect. During the experiments, the initial solution pH was adjusted about 6.5 by negligible volumes of 0.1 M NaOH or HCl solution. As previous preliminary kinetic experiments, one day was sufficient to reach equilibrium [1,27]. Thus, the headspace-free bottles were placed into a thermo stated rotary shaker for one day. To investigate the impacts of pH and IS in a wider parametric range, their ranges were remained wider than those typically used in water and wastewater treatment or discovered in natural water environment. To examine the effect of pH on adsorption, the initial pH (ranging from 3.0 to 12.0) was adjusted with negligible diluted HCl and NaOH solutions without any buffer. To explore the effect of IS, solutions were adjusted with NaCl to the desired levels (IS = 0.001 ~ 0.1 M).

(2) NOM solution experiments: to examine the effect of NOM on rGOs adsorption, these experiments were conducted under preloading condition (representing severe NOM competition) where the addition of NOM was four days prior to spiking estrogens. For the NOM preloading experiments, 1 mg of samples was first stirringly contacted for four days with 3 mg DOC/L NOM solution which was buffered with 1 mM NaH_2PO_4 H_2O/Na_2HPO_4 $7H_2O$ and remained pH 7.0. Afterward, predetermined volumes of each estrogens stock solution were directly spiked into the solutions, and the bottles with free of headspace were then tumbled for an additional day.

After the above isotherm experiments, bottles were placed vertically on a flat surface overnight to allow settling of the adsorbents, and then the supernatants were filtered through 0.22 μm membrane filters to remove the remaining samples. Thereafter, the supernatants were measured using a HPLC (Agilent 1100 Series, USA) which was coupled with a Zorbax 4.6 mm × 150 mm XDB-C8 column (Agilent). The mobile phase make up of methanol/water (v/v, 55:45) at a flow rate of 1 mL/min. The column temperature was adjusted at 30 °C, and the volume of injection was 20 μL. The estrogens was analyzed through the fluorescence detector (excitation wavelength of 280 nm and an emission wavelength of 310 nm) [39,40].

2.5. Date analysis

Four different isotherm models, namely Freundlich (FM), Langmuir (LM), Langmuir-Freundlich (LFM) and Polanyi-Manes models (PMM) [41–44], were used to fit the experimental data. According to the values of determination coefficient (R^2), root mean square error (*RMSE*), and chi-square test (χ^2), FM exhibited good fits for every case (Table S3). Thus, the FM model was chosen to simulate the adsorption data in this article:

$$q_e = K_F C_e^N \quad (1)$$

where q_e (mg/g) is the solid-phase concentration; C_e (mg/L) is the liquid-phase concentration; K_F [(mg/g)/(mg/L)^N] is Freundlich adsorption affinity coefficient; N is Freundlich exponential coefficient related to the surface heterogeneity.

3. Results and discussion

3.1. General characterization

Results of Raman, XRD, and XPS characterizations of the rGOs are shown in Fig. 1. The estimated aromatic matrix size (*L*), content of unoxidized zones in rGOs (*G*%), and content of sp^2 clusters in oxidized zones (*a*%) are calculated in Supporting information and illustrated in Table 1. As could be observed at Table 1, abovementioned three parameters increased with the increase of hydrazine hydrate dose. The oxygen content on rGOs decreased with the increase of reducing agent, which was responsible for the increase of the rGOs pH_{PZC} value with the increasing hydrazine hydrate dose. They all demonstrated that the unoxidized zone in rGOs increased from rGO_1 to rGO_4, while the oxidized zone decreased.

In addition, the surface morphologies of rGOs were examined directly by HR-TEM (Fig. 1D). Results showed that rGOs nanosheet films were transparent and slightly aggregated with the wrinkles loosely located on the basal planes or edges to form groove areas. By increasing the amount of the reducing agent, the crumpled sheets of rGOs became more folded and more serious agglomeration. Furthermore, SSA_{BET}, PV_T and PSD of rGOs are also illustrated in Table 1. rGOs had comparable pore volumes, while SSA_{BET} of rGOs increased with the increase of oxygen content. The measured SSA_{BET} of rGOs were smaller than the theoretically calculated surface area (2630 m^2/g) for monolayer carbon structured graphene [45]. This might be ascribed to aggregation and bundle formation of rGOs and thus resulted in much lower measured SSA_{BET} values (153–342 m^2/g) and the presence of oxidized zone could relieve aggregation and bundle formation [44]. PSD calculated by DFT model exhibited that reduction of graphene material caused an increase in the porosity as a result of tighter aggregation owing to hydrogen bonding between the oxygen containing functional groups within the graphene bundle [46]. Above all, oxidization degree of rGOs was of great influence on their surface structure.

3.2. Influence of adsorbent properties on adsorption of estrogens

Adsorption data of E2 and EE2 onto the rGOs are exhibited in Fig. 2. As seen, with the increase of reduction degree of rGOs, the adsorption capacities of estrogens onto rGOs were enhanced. It is reported that the specific surface area and micropore volumes can account for the adsorption of organic contaminants by microporous adsorbents [47]. As reflected by Fig. S2, the parameters of K_F were negatively correlated with the SSA_{BET} and V_{micro} of the rGOs. This suggested that the specific surface area and micropore volumes of rGOs were not the major contribution factors increased the estrogens uptake. Electrostatic interaction has been proposed to be an adsorption mechanism of ionic organic chemicals onto oxygen-containing carbonaceous adsorbents [31]. At the examined solution pH (6.5), estrogens would not start to deprotonate because of initial solution pH $<$ their pK_a (Table S1). In addition, surfaces of the rGOs would be deprotonated as the initial solution pH was higher than their pH_{pzc} values (Table 1). Thus, electrostatic attraction between the different charged estrogens and rGOs should be responsible for its adsorption. However, electrostatic interaction was unlikely to completely explain the enhanced estrogens adsorption onto rGOs due to adsorption capacities increasing with the increase of reduction degree. Thus, there must be additional mechanisms governing the adsorption. Considering the properties of rGOs and the two selected estrogens, possible interactions can be summarized as follows [48,49]: (i) H-bonding between the estrogens –OH groups and the oxygen-containing functional groups on rGOs; (ii) π–π stacking interaction between π system of rGOs surfaces and the estrogens aromatic moieties.

As reported, H-bonding between functional groups of aromatic organic matters and graphenes is one, but not the major uptake mechanism [38]. In this research, H-bonding was impossible to be the most important factor governing estrogens adsorption onto rGOs for the following reasons: (i) comparison with the H-bonding formed between estrogens and functional groups of rGOs, the formation of water clusters between water molecules and the polar functional groups of rGOs was much stronger [33,50]; (ii) at the investigated solution pH (6.5) over pH_{pzc} of rGOs (Table 1), oxygen-containing functional groups of rGOs would prevail as negatively charged anion and then the rGOs and estrogens might form the negative charge-assisted H-bond [(-)CAHB] [51]. Nevertheless, (-)CAHB contributed little to adsorption in this work due to the negligible pH changes before and after adsorption.

At this point, it seems that only the π–π stacking interaction can be regard as a predominant contribution factor to the increased adsorption capacities of rGOs. Further, the K_F of estrogens was plotted against the reduction degree of rGOs being signed by the surface C/O atomic ratio in Fig. S2. As illustrated, the K_F values were positively correlated with the C/O atomic ratio values of the rGOs. As known, graphene materials have strong adsorption affinity for organics with aromatic ring(s) through the π-electron coupling because of their π-electron-rich characteristic and flat conformation [52]. However, the oxygen-containing functional groups on the surfaces of rGOs might cause delocalization of π electrons from the aromatic matrix, which limited the π–π stacking between the estrogens aromatic moieties and the π system on rGOs. During reduction of GO, the oxygen-containing functional groups on their surfaces was removed substantially, causing the promotion of the π–π stacking between rGOs and estrogens. Thus, π–π stacking interaction could be expected to dominating contribution on the adsorption of estrogens onto rGOs. Moreover, the single point adsorption descriptors, K_d values (q_e/C_e), were also analyzed at different equilibrium concentrations (0.1%, 1%, 10% and 25% C_{sw}) and showed in Table 2. It is clearly that there was a higher adsorption capacity of E2 than EE2 by rGOs, which could be ascribed to the higher hydrophobicity of E2 than EE2 as illustrated by the higher $\log K_{ow}$ value of E2 (Table S1). This indicated that the hydrophobicity of estrogens also affected adsorption capacities on rGOs surface.

3.3. Influence of NOM preloading

The adsorption isotherms of E2 and EE2 by rGOs under NOM preloading are also showed in Fig. 2. Higher R_{K_F} values (the reduction of K_F in the presence of NOM) indicates a higher reduction of adsorption capacity due to the NOM preloading; and the R_{K_F} values are showed in Fig. 3. $K_{d\text{-}NOM}$ (K_d values of adsorption in the presence of NOM) and R_{K_d} (the percent reductions in $K_{d\text{-}NOM}$ values as compared to K_d) were also examined (as illustrated in Fig. 4). As exhibited by Fig. 3, E2 and EE2 uptake by rGOs decreased under NOM preloading, which could be attributed to the following several possibilities: (i) the NOM might directly compete with estrogens for adsorption sites on the surfaces of rGOs driven by π–π and hydrophobic interactions [16]; (ii) the NOM possessing lot of functional groups (i.e. carboxyl, hydroxyl, and amino, etc.) could provide additional sites for forming water clusters through H-bonding after NOM preloading, which consequently affected the hydrophobicity of the adsorbent and then made the hydrophobic sites less accessible to the estrogens [53]; (iii) it is reported that NOM had an average molecular weight ranging from 3700 to 10,500 Da [54], which was sufficiently large to block some of the micropores contributing to the adsorption. Besides, as exhibited R_{K_F} values increased from rGO_1 to rGO_4, the influence of NOM preloading on rGOs adsorption increased with the reduction degree of rGOs increased. On the basis of the properties for both NOM and rGOs, interaction between NOM and rGOs might mainly contribute to π-π stacking between their aromatic moieties [55]. The impacts of NOM were slightly suppressed by the presence of oxygen-containing functional groups on the rGOs, which might be attributed to following two possibilities: (i) the polarity of surface might have better dispersity in water, which decreased the effect of NOM on the target contaminants uptake, and/or (ii) the presence of surface oxygen-containing functional groups restrained the π-π stacking interaction between NOM and rGOs. Moreover, as reflected by Fig. 4,

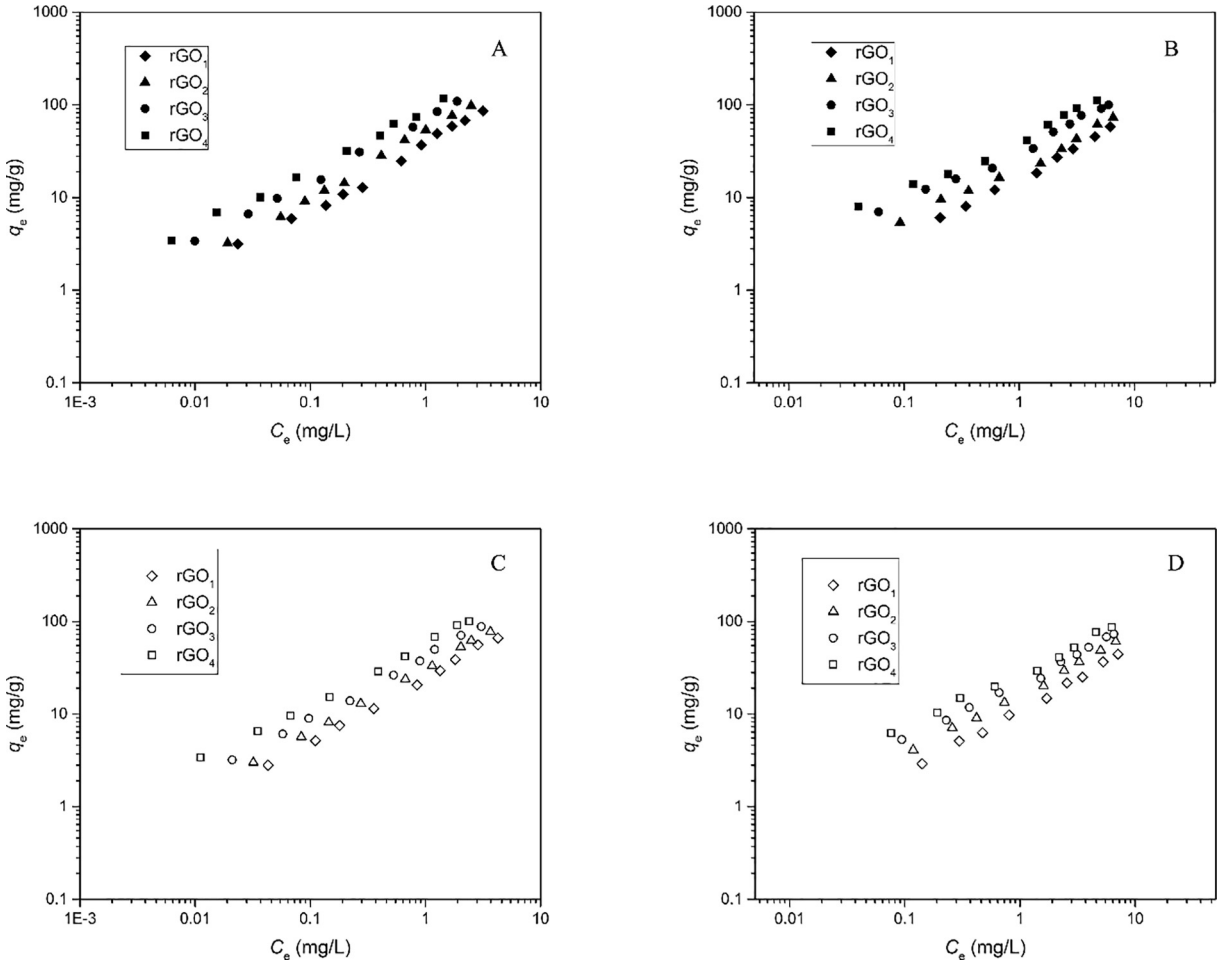

Fig. 2. Adsorption isotherms in ultrapure water (A) E2, (B) EE2 and in NOM solution (C) E2, (D) EE2.

Table 2
K_d value of E2 (A) and EE2 (B) adsorption (calculated at the equilibrium concentration for the corresponding % solubility of each estrogen).

Samples	$K_{d,\ 0.1}$ (L/mg)		$K_{d,\ 1}$ (L/mg)		$K_{d,\ 10}$ (L/mg)		$K_{d,\ 25}$ (L/mg)	
	E2	EE2	E2	EE2	E2	EE2	E2	EE2
rGO_1	0.182	0.055	0.095	0.029	0.050	0.015	0.039	0.012
rGO_2	0.280	0.076	0.140	0.038	0.070	0.019	0.053	0.014
rGO_3	0.412	0.153	0.198	0.070	0.096	0.032	0.071	0.023
rGO_4	0.537	0.213	0.256	0.093	0.122	0.040	0.091	0.029

R_{K_d} decreased with increasing estrogens equilibrium concentrations. This exhibited that displacement of adsorbed NOM molecules would be more difficult when decreasing estrogen concentrations.

As aspect to thermodynamics, adsorption sites of high energy act a crucial role in adsorption, particularly at low adsorbate concentrations [56]. The used NOM concentration of 3.4 mg DOC/L was 2–3 orders of magnitude higher than estrogens at the low concentrations. Hence, the NOM was expected to compete for and took up the high energy adsorption sites, resulting in a decrease of surface heterogeneity. As illustrated by Table S3, the increase in the *N* values of rGOs for E2 was 0.5%–2%, and that for EE2 was 1%–4%. The increasing trends in the *N* values of estrogens uptake on rGOs indicated that NOM molecules tended to adsorbed on the high-energies adsorption sites, making it effective in competition with estrogens. However, small enhancements in the *N* values suggested that the NOM coating did not obviously alter the surface heterogeneity of rGOs.

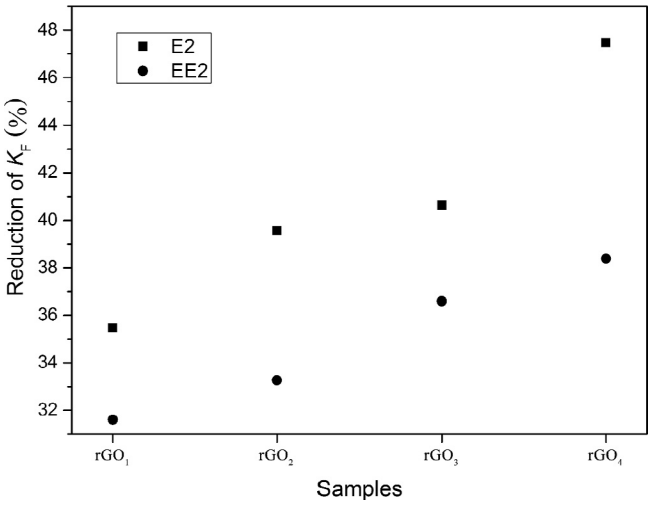

Fig. 3. Percent reduction in K_F of E2 and EE2 adsorption in the presence of NOM when compared to the adsorption under ultrapure water.

3.4. Influence of initial solution pH and IS

Initial solution pH will affect both the surface charge of adsorbents and the speciation distribution of the estrogen contaminants related to their dissociation constants (pK_a). The influence of initial solution pH on the adsorption of E2 and EE2 by rGOs are exhibited in Fig. S3. It is clearly that E2 and EE2 adsorption capacities exhibited slight change

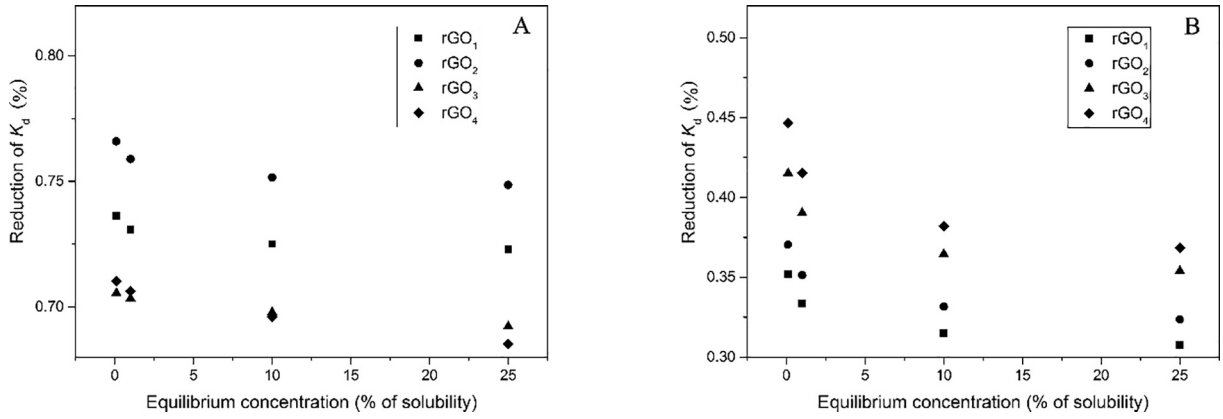

Fig. 4. Percent reduction in K_d of E2 (A) and EE2 (B) adsorption in the presence of NOM when compared to the adsorption under ultrapure water.

with increasing pH up to their p*K*a, followed by a significant decrease of adsorption capacities over their p*K*a. It is reported that higher pH could increase π-electron-donor ability of the aromatic matrix zone of rGOs, which would promote π-π staking interaction between rGOs and estrogens [57]. If the influence of pH on estrogens adsorption was mainly caused by π-π staking interaction, estrogens adsorption would increase with increased pH. However, the opposite trend of estrogens adsorption with pH was observed, ruling out the π–π staking interaction. Thus, the effects of pH on adsorption could be attributed to the possible three aspects: (i) increasing pH might increase the dissociation of the hydrophobic neutral estrogens into hydrophilic and then promoted water cluster formation around the polar sites of rGOs, resulting in decreasing the hydrophobic interaction [58]; (ii) increasing pH would increase the electrostatic repulsion, thus reducing electrostatic attraction between different charged estrogens and rGOs [59]; (iii) increasing pH would decrease H-bonding formation due to the dissociation of functional groups [44].

The variance of the IS can be another important factor which may affect adsorption of estrogens. Fig. S4 exhibits the influence of different IS (NaCl). It has been proposed that organic compounds are less soluble in aqueous salt solutions, which are known as the salting-out effect; salting-out might enhance the hydrophobic interactions of estrogens with rGOs, which was favorable for estrogens adsorption [60]. However, results in Fig. S4 indicated that the amounts of E2 and EE2 adsorbed in rGOs did not increased with an increase in IS. It is also possible that the increase of IS might also change the aggregation state of rGOs. The added ions might penetrate into the diffuse double layer surrounding the rGOs, leading to compression of the diffuse double layer and a reduction in zeta potential. Consequently, repulsive energy between rGOs was reduced, resulting in forming a more compact aggregation structure; this was known as the squeezing-out effect, which was unfavorable for estrogens adsorption [57]. Thus, as reflected by Fig. S4, increasing IS had negligible influence on estrogens uptake by rGOs. This suggested that the contribution of salting-out effect to the estrogens uptake by rGOs was equivalent to that of the squeezing-out effect or both the salting-out effect and squeezing-out effect were too weak to impact the estrogens uptake by rGOs.

4. Conclusions

In this article, the adsorption behavior of estrogens by graphene nanosheets with different reduction degree from water was investigated. Adsorption isotherms followed the order of $rGO_4 > rGO_3 > rGO_2 > rGO_1$, in accordance with the orders of reduction degree. The reduction-induced substantial elimination of oxygen-containing groups from the rGOs surfaces resulted in stronger π–π staking interaction between the rGOs surface and estrogens. In addition, NOM suppressed estrogens adsorption to rGOs; furthermore, more severe NOM influence was found on lower reduction degree because of the presence of surface oxygen-containing functional groups. The represented pH effects on adsorption were correlated with the hydrophobic interaction, electrostatic repulsion, and H-bonding. Changing IS had negligible effect on estrogen adsorption due to the equivalent squeezing-out and salting-out effects.

Acknowledgements

This subject has been supported by the National Natural Science Foundation of China (Grants No. 51521006, 51609268 and 51608208), the Hunan Provincial Innovation Foundation for Postgraduate (Grant No. CX2016B135), and the Key Project of Technological Innovation in the Field of Social Development of Hunan Province, China (Grant Nos. 2016SK2010 and 2016SK2001).

Appendix A. Supplementary data

Supplementary data associated with this article can be found, in the online version, at http://dx.doi.org/10.1016/j.cej.2017.12.034.

References

[1] L. Jiang, Y. Liu, G. Zeng, F. Xiao, X. Hu, X. Hu, et al., Removal of 17β-estradiol by few-layered graphene oxide nanosheets from aqueous solutions: external influence and adsorption mechanism, Chem. Eng. J. 284 (2016) 93–102.
[2] K.S. Novoselov, A.K. Geim, S.V. Morozov, D. Jiang, Y. Zhang, S.V. Dubonos, et al., Electric field effect in atomically thin carbon films, Science 306 (2004) 666–669.
[3] J. Zhang, X. Pan, Q. Xue, D. He, L. Zhu, Q. Guo, Antifouling hydrolyzed polyacrylonitrile/graphene oxide membrane with spindle-knotted structure for highly effective separation of oil-water emulsion, J. Membr. Sci. 532 (2017) 38–46.
[4] X. Li, Q. Xue, X. Chang, L. Zhu, C. Ling, H. Zheng, Effects of sulfur doping and humidity on CO_2 capture by graphite split pore: a theoretical study, ACS Appl. Mater. Interfaces 9 (2017) 8336–8343.
[5] X. Li, Q. Xue, D. He, L. Zhu, Y. Du, W. Xing, et al., Sulfur-nitrogen codoped graphite slit-pore for enhancing selective carbon dioxide adsorption: insights from molecular simulations, ACS Sustain. Chem. Eng. 5 (2017) 8815–8823.
[6] J. Zhang, Q. Xue, X. Pan, Y. Jin, W. Lu, D. Ding, et al., Graphene oxide/polyacrylonitrile fiber hierarchical-structured membrane for ultra-fast microfiltration of oil-water emulsion, Chem. Eng. J. 307 (2017) 643–649.
[7] A. Salehikhojin, D. Estrada, K.Y. Lin, K. Ran, R.T. Haasch, J.M. Zuo, et al., Chemical sensors based on randomly stacked graphene flakes, Appl. Phys. Lett. 100 (2012) 33111.
[8] F. Sharif, L.R. Gagnon, S. Mulmi, E.P. Roberts, Electrochemical regeneration of a reduced graphene oxide/magnetite composite adsorbent loaded with methylene blue, Water Res. 114 (2017) 237–245.
[9] P. Avouris, Graphene: electronic and photonic properties and devices, Nano Lett. 10 (2010) 4285–4294.
[10] C. Fisher, A.E. Rider, Z.J. Han, S. Kumar, I. Levchenko, K. Ostrikov, Applications and nanotoxicity of carbon nanotubes and graphene in biomedicine, J. Nanomater. 2012 (2012) 3.
[11] E.P. Randviir, D.A.C. Brownson, C.E. Banks, A decade of graphene research: production, applications and outlook, Mater. Today 17 (2014) 426–432.
[12] R. Arvidsson, S. Molander, B.A. Sandén, Review of potential environmental and health risks of the nanomaterial graphene, Hum. Ecol. Risk Assess. Int. J. 19 (2013) 873–887.

[13] X. Hu, Q. Zhou, Health and ecosystem risks of graphene, Chem. Rev. 113 (2013) 3815–3835.
[14] K. He, G. Chen, G. Zeng, M. Peng, Z. Huang, J. Shi, et al., Stability, transport and ecosystem effects of graphene in water and soil environments, Nanoscale 9 (2017) 5370–5388.
[15] R.D. Holbrook, N.G. Love, J.T. Novak, Sorption of 17β-estradiol and 17α-ethinylestradiol by colloidal organic carbon derived from biological wastewater treatment systems, Environ. Sci. Technol. 38 (2004) 3322–3329.
[16] L. Jiang, Y. Liu, S. Liu, G. Zeng, X. Hu, X. Hu, et al., Adsorption of estrogen contaminants by graphene nanomaterials under natural organic matter preloading: comparison to carbon nanotube, biochar, and activated carbon, Environ. Sci. Technol. 51 (2017) 6352–6359.
[17] S.D. Kim, J. Cho, I.S. Kim, B.J. Vanderford, S.A. Snyder, Occurrence and removal of pharmaceuticals and endocrine disruptors in South Korean surface, drinking, and waste waters, Water Res. 41 (2007) 1013–1021.
[18] S.U. Akki, C.J. Werth, S.K. Silverman, Selective aptamers for detection of estradiol and ethynylestradiol in natural waters, Environ. Sci. Technol. 49 (2015) 9905–9913.
[19] L. Yang, C. Qiao, N.F. Tam, L. Li, W. Su, T. Luan, Contributions of abiotic and biotic processes to the aerobic removal of phenolic endocrine-disrupting chemicals in a simulated estuarine aquatic environment, Environ. Sci. Technol. 50 (2016) 4324–4334.
[20] L.S. Shore, M. Shemesh, Naturally produced steroid hormones and their release into the environment, Pure Appl. Chem. 75 (2003) 1859–1871.
[21] C. Baronti, R. Curini, G. D'Ascenzo, A. Di Corcia, A. Alessandra Gentili, R. Samperi, Monitoring natural and synthetic estrogens at activated sludge sewage treatment plants and in a receiving river water, Environ. Sci. Technol. 34 (2000) 5059–5066.
[22] X. Bai, R. Feng, Z. Hua, L. Zhou, H. Shi, Adsorption of 17β-estradiol (E2) and Pb(II) on Fe_3O_4/graphene oxide (Fe_3O_4/GO) nanocomposites, Environ. Eng. Sci. 32 (2015) 370–378.
[23] X. Bai, C. Qin, R. Feng, Binary adsorption of 17β-estradiol and bisphenol A on superparamagnetic amino-functionalized graphene oxide nanocomposites, Mater. Chem. Phys. 189 (2017) 96–104.
[24] L.K. Boateng, J. Heo, J.R.V. Flora, Y.-G. Park, Y. Yoon, Molecular level simulation of the adsorption of bisphenol A and 17α-ethinyl estradiol onto carbon nanomaterials, Sep. Purif. Technol. 116 (2013) 471–478.
[25] Y. Wen, Z. Niu, Y. Ma, J. Ma, L. Chen, Graphene oxide-based microspheres for the dispersive solid-phase extraction of non-steroidal estrogens from water samples, J. Chromatogr. A. 1368 (2014) 18–25.
[26] W. Sun, M. Li, W. Zhang, J. Wei, B. Chen, C. Wang, Sediments inhibit adsorption of 17β-estradiol and 17α-ethinylestradiol to carbon nanotubes and graphene oxide, Environ. Sci. Nano 4 (2017) 1900–1910.
[27] L. Jiang, Y. Liu, S. Liu, X. Hu, G. Zeng, X. Hu, et al., Fabrication of β-cyclodextrin/poly (L-glutamic acid) supported magnetic graphene oxide and its adsorption behavior for 17β-estradiol, Chem. Eng. J. 308 (2017) 597–605.
[28] Y. Zhang, S.F. Ali, E. Dervishi, Y. Xu, Z. Li, D. Casciano, et al., Cytotoxicity effects of graphene and single-wall carbon nanotubes in neural phaeochromocytoma-derived PC12 cells, ACS Nano 4 (2010) 3181–3186.
[29] F.F. Liu, J. Zhao, S. Wang, B. Xing, Adsorption of sulfonamides on reduced graphene oxides as affected by pH and dissolved organic matter, Environ. Pollut. 210 (2016) 85–93.
[30] K. Krishnamoorthy, M. Veerapandian, K. Yun, S.J. Kim, The chemical and structural analysis of graphene oxide with different degrees of oxidation, Carbon 53 (2013) 38–49.
[31] Z. Wu, H. Zhong, X. Yuan, H. Wang, L. Wang, X. Chen, et al., Adsorptive removal of methylene blue by rhamnolipid-functionalized graphene oxide from wastewater, Water Res. 67 (2014) 330–344.
[32] J. Wang, Z. Chen, B. Chen, Adsorption of polycyclic aromatic hydrocarbons by graphene and graphene oxide nanosheets, Environ. Sci. Technol. 48 (2014) 4817–4825.
[33] F. Liu, J. Zhao, S. Wang, P. Du, B. Xing, Effects of solution chemistry on adsorption of selected pharmaceuticals and personal care products (PPCPs) by graphenes and carbon nanotubes, Environ. Sci. Technol. 48 (2014) 13197–13206.
[34] H. Hyung, J.-H. Kim, Natural organic matter (NOM) adsorption to multi-walled carbon nanotubes: effect of NOM characteristics and water quality parameters, Environ. Sci. Technol. 42 (2008) 4416–4421.
[35] J.E. Kilduff, T. Karanfil, Trichloroethylene adsorption by activated carbon preloaded with humic substances: effects of solution chemistry, Water Res. 36 (2002) 1685.
[36] H. Wang, Y. Liu, G. Zeng, X. Hu, X. Hu, T. Li, et al., Grafting of β-cyclodextrin to magnetic graphene oxide via ethylenediamine and application for Cr(VI) removal, Carbohydr. Polym. 113 (2014) 166–173.
[37] X. Hu, Y. Liu, H. Wang, G. Zeng, X. Hu, Y. Guo, et al., Adsorption of copper by magnetic graphene oxide-supported β-cyclodextrin: effects of pH, ionic strength, background electrolytes, and citric acid, Chem. Eng. Res. Des. 93 (2015) 675–683.
[38] X. Wang, S. Huang, L. Zhu, X. Tian, S. Li, H. Tang, Correlation between the adsorption ability and reduction degree of graphene oxide and tuning of adsorption of phenolic compounds, Carbon 69 (2014) 101–112.
[39] C. Qin, D. Troya, C. Shang, S. Hildreth, R. Helm, K. Xia, Surface catalyzed oxidative oligomerization of 17β-estradiol by Fe^{3+}-saturated montmorillonite, Environ. Sci. Technol. 49 (2014) 956–964.
[40] L. Joseph, J. Heo, Y.-G. Park, J.R.V. Flora, Y. Yoon, Adsorption of bisphenol A and 17α-ethinyl estradiol on single walled carbon nanotubes from seawater and brackish water, Desalination 281 (2011) 68–74.
[41] Y. Zhou, X. Liu, L. Tang, F. Zhang, G. Zeng, X. Peng, et al., Insight into highly efficient co-removal of p-nitrophenol and lead by nitrogen-functionalized magnetic ordered mesoporous carbon: performance and modelling, J. Hazard. Mater. 333 (2017) 80–87.
[42] Y. Li, X. Yuan, Z. Wu, H. Wang, Z. Xiao, Y. Wu, et al., Enhancing the sludge dewaterability by electrolysis/electrocoagulation combined with zero-valent iron activated persulfate process, Chem. Eng. J. 303 (2016) 636–645.
[43] L. Jiang, S. Liu, Y. Liu, G. Zeng, Y. Guo, Y. Yin, et al., Enhanced adsorption of hexavalent chromium by a biochar derived from ramie biomass (*Boehmeria nivea* (L.) Gaud.) modified with β-cyclodextrin/poly(L-glutamic acid), Environ. Sci. Pollut. Res. (2017) 1–10.
[44] O.G. Apul, Q. Wang, Y. Zhou, T. Karanfil, Adsorption of aromatic organic contaminants by graphene nanosheets: comparison with carbon nanotubes and activated carbon, Water Res. 47 (2013) 1648–1654.
[45] I.A. McAllister, M.J. Li, J.L. Adamson, D.H. Schniepp, H.C. Car, R. Prud'homme, R.K. Aksay, Single sheet functionalized graphene by oxidation and thermal expansion of graphite, Chem. Mater. 19 (2007) 4396–4404.
[46] S. Stankovich, D.A. Dikin, R.D. Piner, K.A. Kohlhaas, A. Kleinhammes, Y. Jia, et al., Synthesis of graphene-based nanosheets via chemical reduction of exfoliated graphite oxide, Carbon 45 (2007) 1558–1565.
[47] G. Newcombe, J. Morrison, C. Hepplewhite, D.R.U. Knappe, Simultaneous adsorption of MIB and NOM onto activated carbon: II Competitive effects, Carbon 40 (2002) 2147–2156.
[48] J. Björk, F. Hanke, C.A. Palma, P. Samori, M. Cecchini, M. Persson, Adsorption of aromatic and anti-aromatic systems on graphene through $\pi-\pi$ stacking, J. Phys. Chem. Lett. 1 (2010) 3407–3412.
[49] A. Rochefort, J.D. Wuest, Interaction of substituted aromatic compounds with graphene, Langmuir 25 (2008) 210–215.
[50] A. Irena Efremenko, M. Sheintuch, Predicting solute adsorption on activated carbon: phenol, Langmuir 22 (2006) 3614–3621.
[51] M.B. Ahmed, J.L. Zhou, H.H. Ngo, W. Guo, M.A.H. Johir, K. Sornalingam, Single and competitive sorption properties and mechanism of functionalized biochar for removing sulfonamide antibiotics from water, Chem. Eng. J. 311 (2017) 348–358.
[52] M. Sander, J.J. Pignatello, Characterization of charcoal adsorption sites for aromatic compounds: insights drawn from single-solute and bi-solute competitive experiments, Environ. Sci. Technol. 39 (2013) 1606–1615.
[53] L. Lou, F. Liu, Q. Yue, F. Chen, Q. Yang, B. Hu, et al., Influence of humic acid on the sorption of pentachlorophenol by aged sediment amended with rice-straw biochar, Appl. Geochem. 33 (2013) 76–83.
[54] R. Baigorri, M. Fuentes, G. Gonzalez-Gaitano, J.M. García-Mina, Simultaneous presence of diverse molecular patterns in humic substances in solution, J. Phys. Chem. B 111 (2007) 10577–10582.
[55] J. Zhang, J.-L. Gong, G.-M. Zenga, X.-M. Ou, Y. Jiang, Y.-N. Chang, et al., Simultaneous removal of humic acid/fulvic acid and lead from landfill leachate using magnetic graphene oxide, Appl. Surf. Sci. 370 (2016) 335–350.
[56] S. Yang, J. Li, D. Shao, J. Hu, X. Wang, Adsorption of Ni (II) on oxidized multi-walled carbon nanotubes: effect of contact time, pH, foreign ions and PAA, J. Hazard. Mater. 166 (2009) 109–116.
[57] O.G. Apul, T. Karanfil, Adsorption of synthetic organic contaminants by carbon nanotubes: a critical review, Water Res. 68 (2015) 34–55.
[58] D. Lin, B. Xing, Adsorption of phenolic compounds by carbon nanotubes: role of aromaticity and substitution of hydroxyl groups, Environ. Sci. Technol. 42 (2008) 7254–7259.
[59] B. Pan, B. Xing, Adsorption mechanisms of organic chemicals on carbon nanotubes, Environ. Sci. Technol. 42 (2009) 9005–9013.
[60] J.C. Lazo-Cannata, A. Nieto-Márquez, A. Jacoby, A.L. Paredes-Doig, A. Romero, M.R. Sun-Kou, et al., Adsorption of phenol and nitrophenols by carbon nanospheres: effect of pH and ionic strength, Sep. Purif. Technol. 80 (2011) 217–224.